論文 / 著書情報
Article / Book Information

Title	Extraordinary transmission of gold-capped sphere arrays in mid-infrared range
Authors	Hoang Thi Thanh Tam, Kotaro Kajikawa
Citation	Optics Express, Vol. 29, Issue 22, pp. 35191-35205
Pub. date	2021, 10
Copyright	(c) 2021 Optica Publishing Group. Users may use, reuse, and build upon the article, or use the article for text or data mining, so long as such uses are for non-commercial purposes and appropriate attribution is maintained. All other rights are reserved.
DOI	http://dx.doi.org/10.1364/OE.439357

Research Article | Vol. 29, No. 22 / 25 Oct 2021 / Optics Express 35191
Optics EXPRESS

Extraordinary transmission of gold-capped sphere arrays in mid-infrared range

HOANG THI THANH TAM AND KOTARO KAJIKAWA*

School of Engineering, Department Electrical and Electronic of Engineering, Tokyo Institute of Technology, Nagatsuta, Midori-ku, Nagatuda, Yokohama 226-8502, Japan
kajikawa@ee.e..titech.ac.jp

Abstract: We report an extraordinary transmission (EOT) of gold-capped silica microsphere monolayers in the mid-infrared range of 5–25 μm. The observed transmittance is significantly greater than that of a flat gold film with the same thickness, although the surface of the microsphere monolayer appeared to be completely covered with gold when observing from above. The calculations based on the finite difference time domain method indicate that light passes through the openings between the gold coating on the substrate and that on the microspheres. The EOT-type studied here occurs over the mid-infrared wavelength range, thus indicating that it is not attributable to the resonance of the surface plasmons. This type of EOT is absent in the visible and near infrared wavelength range, where gold does not function as an ideal metal. In addition, spectral modification originating from localized phonon polariton resonance (LPhPR) in silica microsphere is observed. LPhPR can be interpreted based on the analogy of the localized surface plasmon resonance in metallic nanospheres, in the visible or ultraviolet wavelength range.

1. Introduction

Dielectric microspheres are sometimes self-assembled on a substrate to form two-dimensional crystals. When microspheres are capped with noble metal films, interesting optical properties emerge. A successful application of this structure is in the surface-enhanced Raman scattering (SERS) spectroscopy [1–5]. Intense electric fields of light are produced in the spaces between the microspheres, resulting in an extremely enhanced SERS signal. Another application is in sensitive optical sensors [6–12], based on the property that the resonance condition of the localized surface plasmons produced in the metal-capped microspheres is sensitive to the refractive index variation of the ambient medium. Other studies have been conducted on photoemission electron microscopy [13] and optical properties [14–17], as well as numerical simulations [18,19].

Extraordinary transmission (EOT) is a phenomenon in which the light transmittance is greater than that expected from the proportion of the hole or gap area in a metallic film [20–23]. EOT occurs in a narrow wavelength range, thus suggesting that it emerges from surface plasmon resonance. Hence, it is usually observed in periodically arranged arrays, such as two-dimensional hole-arrays and slits. EOT phenomena are also reported in metal-capped microsphere crystals [24,25]. When the microspheres form periodic structures in order of the light wavelength, the EOT may exhibit a similar mechanism to that of ordered holes in a metallic film. This interpretation is supported by abrupt EOT peaks in the transmission spectra. Although these studies are carried out for visible or near-infrared (IR) light, the EOT at mid-IR range, which is important in vibration spectroscopy and black-body radiation, remains unclear. To our knowledge, one paper has reported EOT using a periodically perforated silicon-dioxide film at mid-IR wavelengths [26], in which the transmission spectrum has a sharp peak.

In this paper, we report the broadband EOT phenomena in gold-capped silica (Au-SiO_2)-microsphere and gold-capped polystylene (Au-PS)-microsphere monolayers, in the mid-IR range (5–25 μm). High transmittance was observed over the mid-IR range, although the surface appears to be completely covered with gold when observing from above. Light passes through

#439357 https://doi.org/10.1364/OE.439357
Journal © 2021 Received 3 Aug 2021; revised 30 Sep 2021; accepted 1 Oct 2021; published 13 Oct 2021

Optics EXPRESS

the openings between the gold coating on the substrate and that on the microspheres. The EOT is observed in a wide wavelength range, which suggests that it is free from the resonance phenomenon. Numerical calculations based on the finite difference time domain (FDTD) method was performed to reveal the EOT mechanism.

2. Experiments and calculation

Figures 1(a) and 1(b) present the schematics of the Au-SiO_2 monolayer and its preparation process, respectively. Silica (SiO_2) microspheres were immobilized on a silicon substrate using an adhesive monolayer of a silane-coupling agent, and a 25-nm thick gold film was vacuum-evaporated onto the microsphere monolayers.

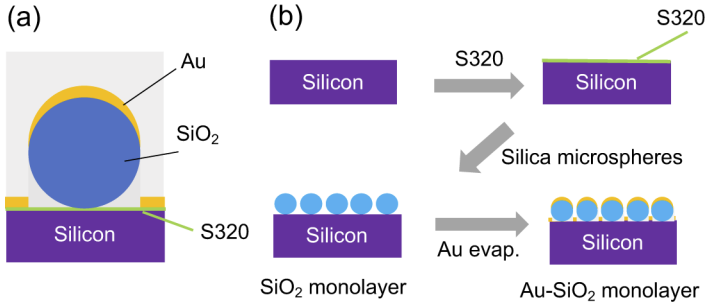

Fig. 1. (a) Schematic illustration of a SiO_2 microsphere monolayer and (b) its fabrication process.

The colloidal SiO_2-bead suspension (sicastar, MPT, Germany) was adopted to form the microsphere monolayer. Their diameters, ϕ, were 0.3, 1, and 3 μm. The solid content of the solution was 50 mg/ml. The colloidal suspensions were diluted with pure water at a certain ratio (1/10, $1/10^3$, or $1/10^5$) to control the density of the SiO_2 microspheres on a substrate. The substrate was a 0.53-mm thick silicon wafer (P-type, high resistance, crystal orientation: 100) with a dimension of 25×25 mm^2. They were cleaned by sonication in an aqueous solution of Extran MA 02 (Merk), pure water, isopropanol, and acetone. The substrate surface was modified with an silane-coupling agent of N-(2 aminoethyl)-3-aminopropyltrimethoxysilane, $H_2N(CH_2)_2NH(CH_2)_3Si(OMe)_3$ (S320, Sila-Ace, JNC). The S320 monolayer was formed by the immersion of the substrate for 1 h in a mixture solution of an acetic acid/ethanol (5: 95 v/v), at a volume concentration of 1.1%. The substrates were rinsed with ethanol, and were immediately immersed in the SiO_2 colloidal solution for 1 h, to form a SiO_2-microsphere monolayer. Finally, the substrates were rinsed with deionized water to remove excess SiO_2 microspheres, and were dried at room temperature. The SiO_2-microsphere monolayer was coated with a 25-nm thick gold thin film via thermal vacuum-evaporation.

For high-coverage Au-PS-microsphere monolayers, the PS bead solution was mixed with ethanol at a mixing volume ratio of 1:3. In the ethanol solution, 0.2 v% of Triton X was added as a surfactant. The PS bead solution was centrifuged at 6500 rpm for 10 min. Subsequently, 42.5% of the solvent was removed from the solution. Then the solution was stirred again via sonication. A mixed PS solution (30 μL) was dropped on a silicon substrate and spin-coated at 1000 rpm for 6 s. Medium and low coverage Au-PS microsphere monolayers were prepared on a silicon substrate covered with a self-assembled monolayer (SAM) of S320. The PS bead solution was diluted with pure water at the mixing volume of 1:49 and 1:24 for medium and low coverage, respectively. Then, the PS solution was dropped on the substrate, followed by a 30-min wait. Excess PS particles were removed by rinsing the substrate in pure water and 2-propanol. Finally, the sample was dried at room temperature before a gold film was deposited.

Optics EXPRESS

IR transmittance spectra were obtained with a Fourier-transmission infrared spectrometer (FT/IR-4600, JASCO). The spectral range was from 400 cm^{-1} to 4000 cm^{-1}, with a resolution of 2 cm^{-1}. The collimated infrared light is normally incident to the sample with no focusing. The corresponding wavelength range is 2.5–25 μm. The spot aperture size was 5 mm in diameter. A silicone plate was adopted as a reference to measure the baseline. The monolayer was observed via scanning electron microscopy (SEM) with JSM-6610A (JEOL), and the surface coverage of the microspheres was evaluated by SEM images, using the ImageJ software (National Institutes of Health, USA) [27–29].

To elucidate the mechanism of the EOT, electromagnetic field analysis was performed using a FDTD software (Full WAVE, Synopsys Inc.). The Yee mesh size in the x, y, and z-direction was $10 \times 10 \times 5$ nm^3. The periodic boundary condition was applied in the x and y-directions, as well as the perfectly-matched-layer condition in the z-direction, where the z-direction is along the surface normal. The dielectric constant of silica was taken the literatures presented by Malitson [30] and Kitamura [31] to cover the wide wavelength range, from ultraviolet to mid-IR. The dielectric constant of PS is taken from the literatures [32,33]. The dielectric constant of gold is taken from the literature presented by Olmon [34]. The dielectric constants were installed in the FDTD software.

3. Results and discussion

3.1. Experiments

3.1.1. SiO_2- and Au-SiO_2-microsphere monolayers

Figure 2 presents SEM images of the Au-SiO_2-microsphere monolayers. The diameter of the microspheres and the thickness of the gold coating were 1 μm and 25 nm, respectively. The Au-SiO_2-microsphere monolayers with three different microsphere coverages were prepared by altering the dilution ratio of the colloidal suspension: (a) 1/10, (b) $1/10^3$, and (c)$1/10^5$, respectively. The mean coverages, σ, evaluated from the SEM images were 0.87, 0.25 and 0.04. At the highest coverage, (a), the microspheres are ordered, and they form two-dimensional crystals. At $\sigma = 0.25$, (b), the microspheres form linear aggregates and the distance between the aggregates are ~ 10 μm. At a low coverage ($\sigma = 0.04$), (c), most microspheres are isolated, and some from dimers or trimers.

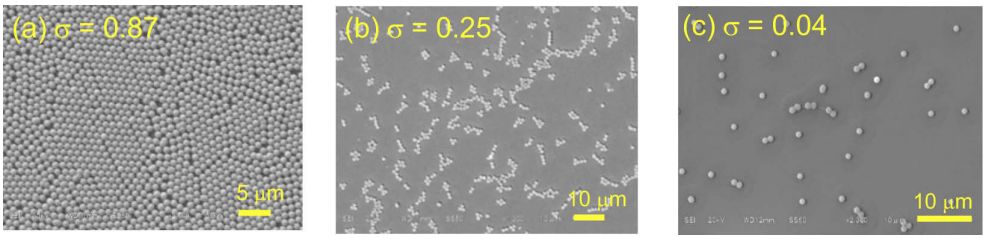

Fig. 2. SEM images of the Au-SiO_2 microsphere monolayers.

The transmittance spectra of the Au-SiO_2- and SiO_2-microsphere monolayers are presented in Fig. 3. The baseline was taken with a silicone plate that was used as a substrate. The transmittance was evaluated as the ratio of the light intensity transmitted through the sample to that of the silicone plate. The coverages of the microspheres are 0.87 and 0.86, respectively. The transmittance spectra of a 25-nm thick flat gold film was also measured. The SiO_2-microsphere monolayer has a transmittance approximately 100% over the wavelength ranges, except for the wavelengths of the localized phonon polariton resonance (LPhPR), at 9 and 21 μm, which will be discussed later. The transmittance, T, is higher than 100% at the wavelengths from 3 to 7.5 μm,

Optics EXPRESS

as it functions as an antireflection coating and reduces the reflectance at the silicone surface. The Au-SiO_2-microsphere monolayer has a transmittance approximately 60% over the wavelength range of 5–25 μm, except for the wavelengths of the LPhPR, although the surface was fully covered with a 25-nm thick gold film. A 25-nm thick flat gold film has a transmittance less than 1.5% over this wavelength range, which is significantly less than that of the Au-SiO_2-microsphere monolayer. These results imply that the gold coating does not prevent the light transmission at the wavelengths. In a previous report [25], the EOT is observed in a narrow wavelength range of near-IR. The high transmittance observed in this study has no peak, which indicates a different EOT mechanism. The low transmittance at wavelengths shorter than 5 μm stems from the imaginary permittivity of gold at this wavelength range. This also triggers the slight increase in the transmittance spectra of the flat gold film at this wavelength range.

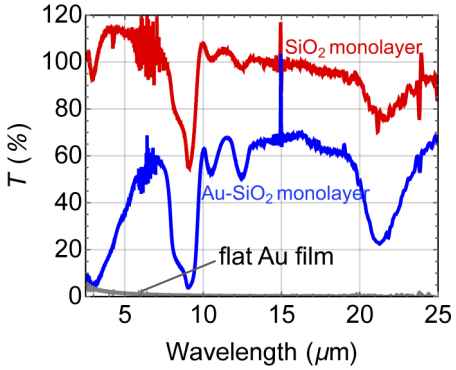

Fig. 3. Transmittance spectra of the SiO_2- and Au-SiO_2-microsphere monolayers 1-μm in diameter. Both coverages of the microspheres are approximately the same ($\sigma \sim 87\%$).

The observed dips at 9 and 21 μm in the transmittance spectra stem from the LPhPR [35]. It originates from the negative real-permittivities of SiO_2. Real and imaginary permittivities of silica are plotted in Fig. 4(a), with resonances at 9 and 21 μm, respectively, where imaginary permittivity has a peak and the real permittivity is negative. Figure 4(b) presents the absorption cross-section, C_{abs}, of silica microsphere with a 1-μm diameter, calculated as a function of the wavelength, based on the Mie theory. This LPhPR appears as two absorption cross-section peaks at 8.5 and 20.5 μm. The LPhPR wavelengths correspond to those at which the real permittivity is equal to -2, by analogy to the localized surface plasmons in metallic nanospheres, under the quasi-static approximation.

3.1.2. Coverage dependence

Figure 5(a) presents the transmittance spectra of Au-SiO_2-microsphere monolayer with different coverages, σ. At $\sigma = 0.87$, the transmittance is highest (approximately 60%), and at $\sigma = 0.25$ and 0.04, it is approximately 15% and 3%, respectively. The transmittance decreases with a decrease in the coverage, indicating that the light is transmitted through the gold-capped microspheres. The transmittance normalized by the coverage, T/σ, is also plotted in Fig. 5(b), to evaluate the transmittance through the microsphere, because the transmittance of the flat gold films on the substrate is negligible. Even in the normalized transmittance spectra, the transmittance decreases with a decrease in the coverage. This means that the transmittance is not proportional to the number of microspheres.

3.1.3. Au-PS-microsphere monolayer

We also measured the transmission spectra of the Au-PS-microsphere monolayers, to present the EOT with no LPhPR. We prepared Au-PS-microsphere monolayers ($\phi = 0.25$ μm) with coverages

Optics EXPRESS

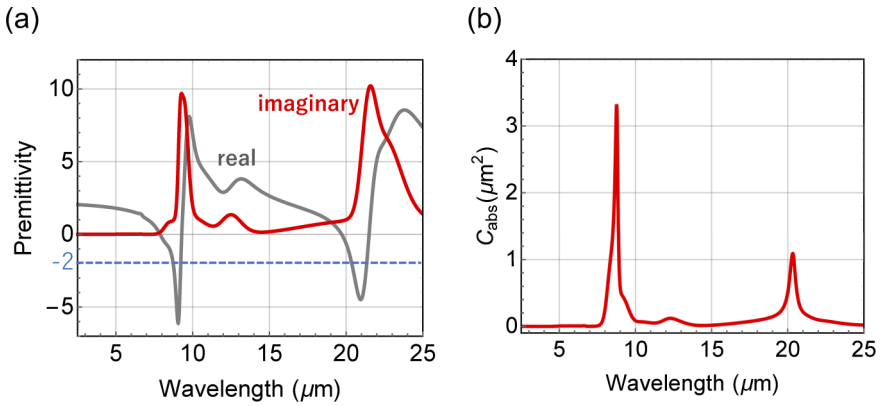

Fig. 4. (a) Permittivity of silica and (b) Absorption cross-section of silica spheres of 1 μ diameter. The LPhPR occurs at the wavelength of the real permittivity equal to -2.

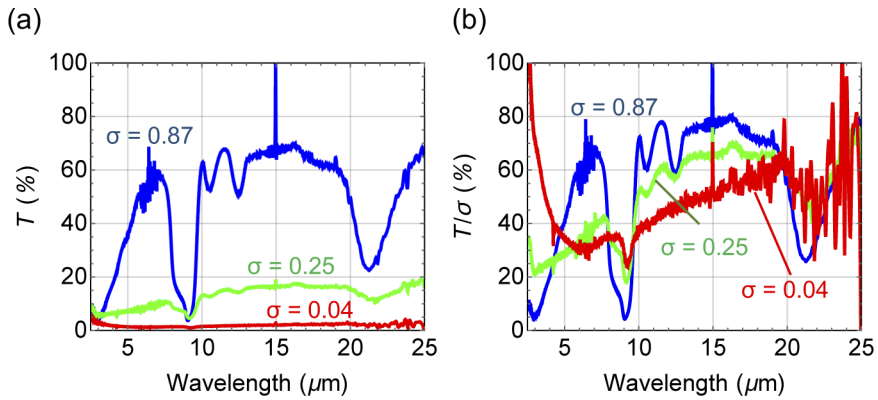

Fig. 5. (a) Transmittance spectra of the Au-SiO_2-microsphere monolayers with different coverages, σ, and (b) their transmittance spectra normalized by the coverages.

of σ = 0.65, 0.34, and 0.10. The SEM images are presented in Fig. 6. The microspheres form two-dimensional crystals at σ = 0.65, and they are isolated in the Au-PS-microsphere monolayers at σ = 0.30 and 0.10. The coverages are similar to those of the Au-SiO_2-microsphere monolayers, as discussed above.

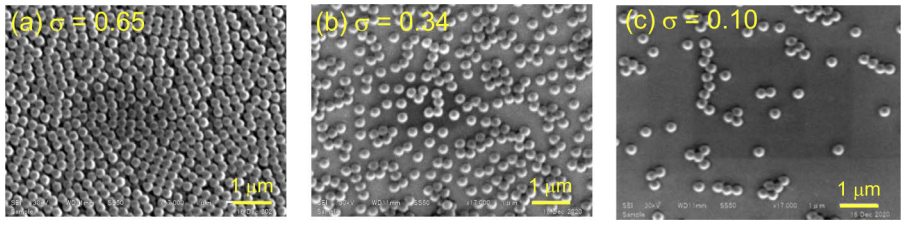

Fig. 6. SEM images of the Au-PS-microsphere monolayers at various coverages, σ.

The transmittance spectra of the Au-PS-microsphere monolayers are presented in Fig. 7(a), together with the spectra of a 25-nm thick flat gold film. The transmittance is almost constant with no peaks, and is approximately 60%, 25%, and 6% for σ = 0.65, 0.34, and 0.10, respectively.

Optics EXPRESS

The corresponding transmittance normalized by the coverage is presented in Fig. 7(b). Similar to the results of the Au-SiO_2-microsphere monolayers, the normalized transmittance of the Au-PS-microsphere monolayers decreases with decreasing coverage. The EOT observed in the Au-PS-microsphere monolayers without any dips suggests that the EOT observed in this study is not due to LPhPR. This is supported by the FDTD calculation below.

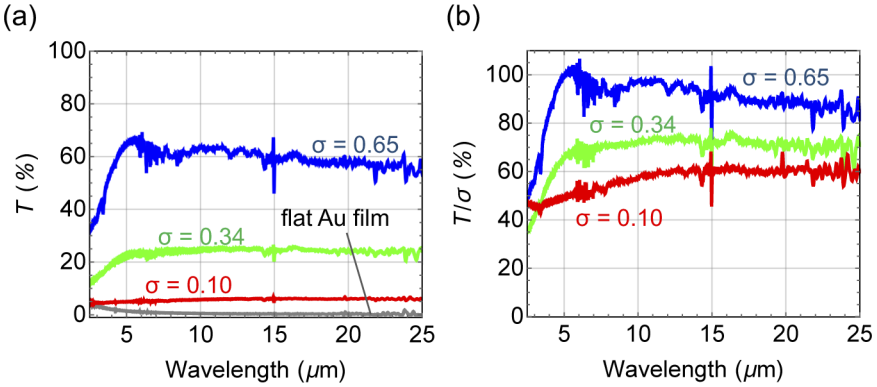

Fig. 7. (a) Transmittance spectra of the Au-PS-microsphere monolayers with various coverages, σ and (b) their normalized transmittance spectra.

3.1.4. Size dependence

Transmittance spectra of the Au-SiO_2-microsphere monolayers comprising different microsphere sizes were examined. Figure 8 presents their SEM images. The monolayer (ϕ = 0.3 and 1 μm) consists of two-dimensional crystals, and the microspheres are attached, whereas the microspheres in the monolayer (ϕ = 3 μm) are not ordered well, and the microspheres are separated with gaps, resulting in the lower coverage. This low order may be triggered by the large deviation of the microsphere sizes. The transmittance spectra of the Au-SiO_2-microsphere monolayers are presented in Fig. 9(a), and the spectra normalized by the coverages are presented in Fig. 9(b). The ordered monolayers of (ϕ = 0.3 and 1 μm) have a high transmittance, whereas that of ϕ = 3 μm is low approximately 30%, even in the normalized spectrum. This low transmittance at ϕ = 3 μm is owing to the gaps between the microspheres, as discussed in the next session, based on the FDTD calculations.

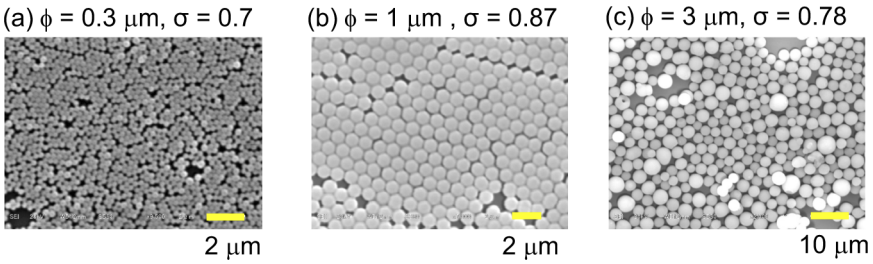

Fig. 8. SEM images for the Au-SiO_2-microsphere monolayers of different microsphere diameters.

Optics EXPRESS

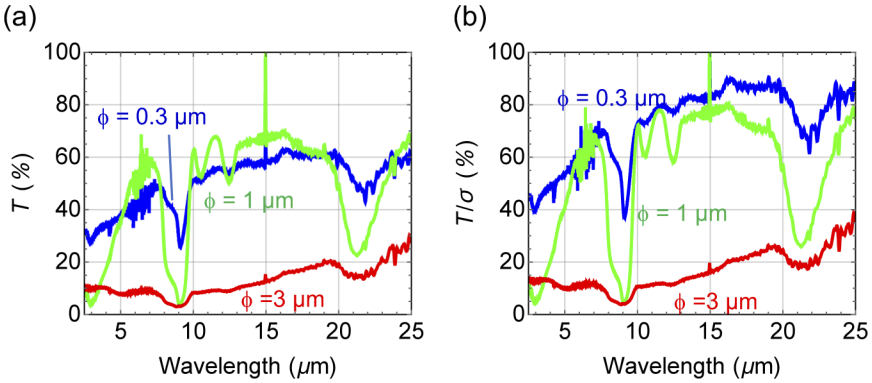

Fig. 9. (a) Transmittance spectra for the Au-SiO_2-microsphere monolayers of different diameters, and (b) their transmittance spectra normalized by the coverage, σ.

3.2. FDTD calculation

3.2.1. SiO_2-, Au-SiO_2- and Au-PS-microsphere monolayers

To investigate the EOT mechanism, we modeled the SiO_2- and Au-SiO_2-microsphere monolayers, where the microspheres form a square lattice, with a lattice constant equal to the microsphere diameter at $\phi = 1$ μm. Then, the coverage is $\sigma = \pi/4$ =0.79. First, we demonstrate the transmittance spectra of the SiO_2- and the Au-SiO_2-microsphere monolayers in Fig. 10(a). The gold film thickness to cap the microsphere was set to be 25 nm. The corresponding experimental spectra are presented in Fig. 3. In the mid-IR region (5 – 25 μm), a high transmittance is observed for both structures, except for the LPhPR dips at 9 and 21 μm. The absolute transmittance almost agrees with the experimental results, as presented above. Hence, the FDTD calculation optimally reproduce the experimental results.

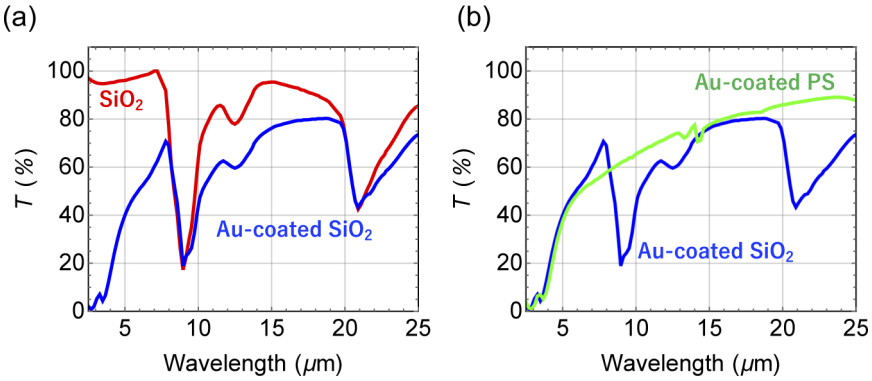

Fig. 10. (a) Calculated transmittance spectra of the SiO_2- and Au-SiO_2-microsphere monolayers 1-μm in diameter. (b) Calculated transmittance spectra of the Au-SiO_2- and Au-PS-microsphere monolayers 1-μm in diameter.

Figure 10(b) presents calculated transmittance spectra of the Au-SiO_2- and Au-PS-microsphere monolayers 1-μm in diameter. The transmission spectra are almost similar except for the wavelengths of the LPhPR regions of SiO_2 at 9 and 21μm. In the experimental transmittance spectra of the Au-PS-microsphere monolayers (Fig. 7(a)), the dips stemming from the LPhPR are absent. Thus, we can conclude that the LPhPR does not play a role in the EOT observed in this study.

Optics EXPRESS

3.2.2. Size dependence

We present the transmittance spectra calculated for the Au-SiO_2-microsphere monolayers of different diameters, ϕ, in Fig. 11(a). The corresponding experimental results are presented in Fig. 9. To compare the calculated spectra with the experimental results, the spectra were normalized by the coverage, as illustrated in Fig. 11(b). It is obvious that the transmittance decrease with the size of the microsphere, even in the normalized spectra. This results does not agree with the experimental results, in which the Au-SiO_2-microsphere monolayers at $\phi = 0.3$ μm are similar to that at $\phi = 1$ μm, in the normalized transmittance spectra in Fig. 9(b). The difference may be triggered by the low coverage of the Au-SiO_2-microsphere monolayer ($\phi = 0.3$ μm), where the microsphere crystals are separated, and low order of the microspheres ($\phi = 3$ μm).

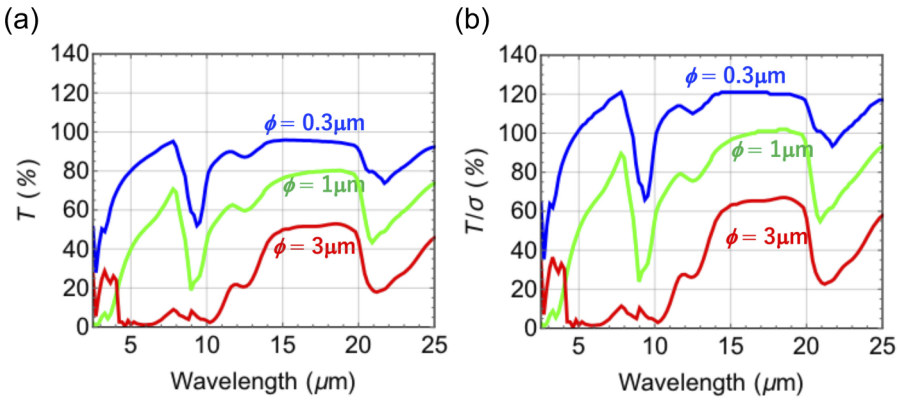

Fig. 11. (a) Calculated transmittance spectra of the Au-SiO_2-microsphere monolayers with various sizes $\phi = 0.3, 1$, and 3 μm and (b) their transmittance spectra normalized by the coverage, σ.

The decrease in transmittance with the size of the microsphere suggest that light is transmitted along the surface of the gold-capped microspheres (outer circumference), rather than through the entire microspheres. Consider the top-view of a microsphere monolayer forming a square lattice. The surface number density of the microsphere, N, in a square lattice is written as $N = 1/(4r^2)$, where r is a diameter of the microspheres relative to the unit length. The surface area of the microsphere is constant at $\pi/4$, and is independent of the microsphere size. In contrast, the length of the microsphere circumference, L, is $L = \pi/(2r)$, indicating that L increases with decreasing r. Considering the results in which transmittance increases with decreasing size, it is suggested that the light propagates along the microsphere circumference. For instance, light passes through the gaps between the gold film on the substrate and that on the microspheres; hence the transmittance is higher as microspheres are smaller. This picture is supported by the temporal variation of the electric field calculated by the FDTD calculation, as described below.

3.2.3. Coverage dependence

We present the transmittance spectra of the Au-SiO_2-microsphere monolayers ($\phi = 1$ μm) with different inter-sphere gaps, g, in Fig. 12(a). The models with six different gaps were examined. The spheres are attached at $g = 0$. The transmittance T decreases with the increase in the gap distance g over the spectral range. The low transmittance is not solely owing to the low coverage of the microspheres. To validate this statement, we present the transmittance normalized by the coverage, σ, in Fig. 12(b). Even normalized transmittance decreases with σ, indicating that the transmittance is significantly affected by the gap distance.

Optics EXPRESS

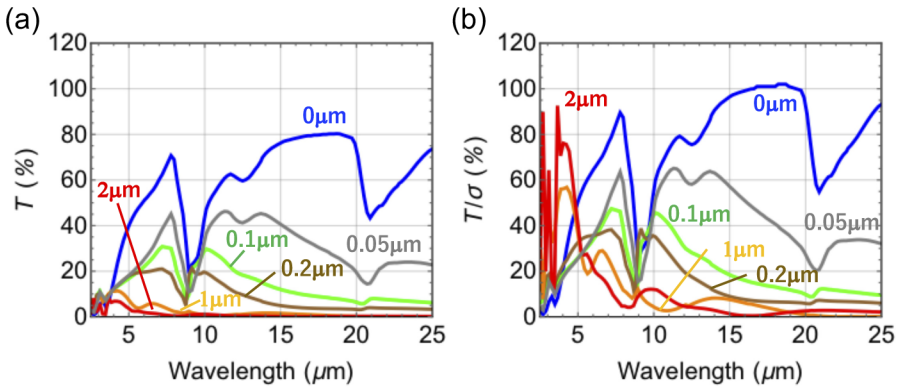

Fig. 12. (a) Calculated transmittance spectra of the samples with various inter-particle distances, and (b) their transmittance spectra normalized by the coverage, σ.

Figure 13 plots calculated and measured transmittance, T, as a function of coverage σ at 16 μm, where the silica microsphere is free from the LPhPR. The measured transmittance is taken from the Fig. 5. The calculated and measured transmittance are discrepant, particularly at low coverage. This is owing to the aggregation of the microspheres in the Au-SiO_2-microsphere monolayers at σ = 0.25 and 0.04, as presented in the SEM images of Figs. 2(b) and 2(c). In the calculation models, the microspheres are isolated. Aggregated microspheres exhibit higher transmittance than those of isolated microspheres.

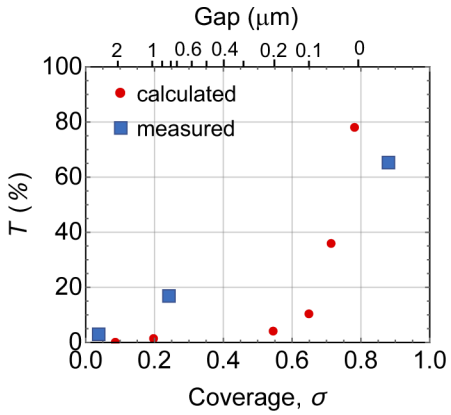

Fig. 13. Calculated and measured transmittance at a wavelength of 16 μm, T, as a function of coverage σ and the gap distance.

3.2.4. Gold thickness dependence

The calculated transmittance spectra of the Au-SiO_2-microsphere monolayers (ϕ = 1 μm) with different gold thickness, d, are presented in Fig. 14. With increasing the gold thickness, the transmittance gradually decreases, and it is greater than 40% even for the thick gold film at d = 45 nm. The transmittance of the Au-SiO_2-microsphere monolayers with $d \geq$ 50nm are significantly lower than the others at wavelengths longer than 5 μm. This may be due to gold clogging up the spaces between the gaps and the gold caps become continuous with low resistivity. Details are under investigation and will be reported elsewhere.

Optics EXPRESS

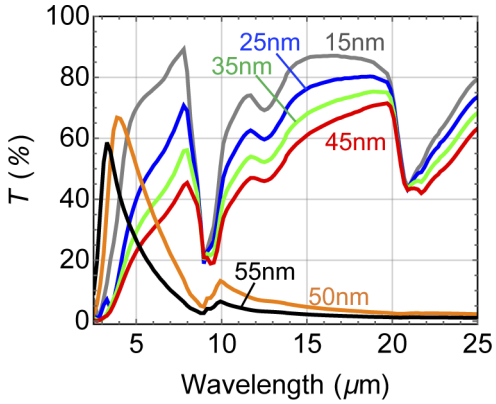

Fig. 14. Calculated transmittance spectra of the Au-SiO_2-microsphere monolayers (ϕ = 1 μm) with different gold thicknesses, d.

3.2.5. Gap between microspheres

To investigate the EOT, the transmittance spectra of two models are calculated. Model 1a is an Au-SiO_2-microsphere monolayer on a silicone substrate. The microspheres are attached, i.e., g = 0, as shown in Fig. 15(a). The thickness of the gold coating is 25 nm. Model 1b is a 25-nm-thick gold film with 1-μm diameter holes. Model 1b is the geometry of Model 1a without the spheres. The surface appears to be covered with gold when observed from the top. The side view is the cross-sectional view containing the points where the spheres are in contact. Gold was absent on this cross-sectional plane, although thin diamond-shaped gold films exist on the silicone substrate.

The calculated spectra of Model 1a and 1b are presented in Fig. 15(b). Model 1b has a high transmittance over the mid-IR range, although the coverage of the thin diamond-shaped gold films is calculated as 21%. This means that the light is transmitted through the circular gaps between the diamond-shaped gold films, because each diamond-shaped gold film is isolated. We previously reported a similar EOT phenomenon via metallic grating, in the IR range [36].

Figure 15(c) presents the top and side view of the Model 2a with g = 0.05 μm. In contrast to Model 1, the gold film on the substrate is continuous and contains holes, and thus the transmittance is low. The calculated spectra of Models 2a and 2b are presented in Fig. 15(d). The transmittance of Model 2b monotonically decreases with the wavelength. The transmittance of Model 2b is higher than that of Model 2a at a wavelength range longer than 10 μm. In this wavelength region, the gold-capped SiO_2 microspheres promotes the transmission, and the transmittance of Model 2a is greater than that of the Model 2b. This means that the gold-capped silica spheres function as light collectors to collect the light and allow it to pass through the hole, thereby resulting in a greater transmittance.

3.2.6. Electric field distribution

Temporal variations in the electric field distribution are calculated via the FDTD method at a wavelength of 16 μm, where the silica microspheres are free from the LPhPR effect. We present the top and side views of the model for the calculation in Fig. 16(a). The calculation model is the Au-SiO_2-microsphere monolayer forming a square lattice, where the microspheres are attached (g = 0 μm). The absolute value of the incident field was set to be unity.

We present both electric field distributions in the cut plane including AB and CD. The electric field is enhanced at the point where the spheres are attached, and the light is transmitted as in the electric field distribution map of the cut plane including AB. The white parts at the boundary

Optics EXPRESS

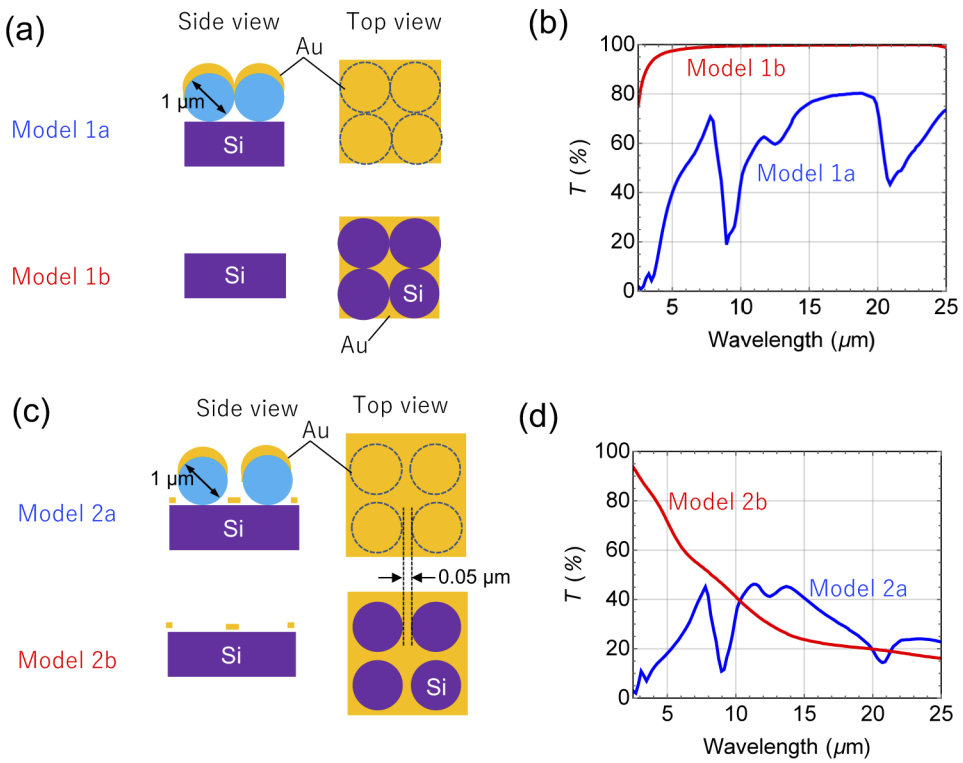

Fig. 15. (a) Schematic drawing of Model 1, where the microspheres are attached ($g = 0$). Model 1b is Model 1a without the microspheres. (b) Transmittance spectra of Models 1(a) and 1(b). (c) Schematic drawing of Model 2, where the microspheres are separated with a gap of 0.05 μm. Model 2b is Model 2a without the microspheres. (d) Transmittance spectra of Model 2(a) and 2(b).

(indicated by arrows) represent the electric field grater than 6, and the maximum electric field is calculated to be approximately 18. The electric field behind the gold cap is negligibly weak owing to the low transmittance of the gold film capping the microspheres. Hence, we infer that light passes through the gaps and openings between the gold-capped microspheres.

The electric field distributions in the cut plane with CD, where spheres are not in contact, are also illustrated. Even in this model, light is transmitted in a direction along the microsphere surface. These phenomena are not observed for the model with no gold caps, i.e., SiO_2-microsphere monolayer. Therefore, the gold cap plays an important role in the EOT. Figure 16(b) presents the electric field distribution of Au-SiO_2-microsphere monolayer that has a gap of $g = 0.05$ μm. The enhancement of the electric field is weaker than that of Au-SiO_2-microsphere monolayer with a gap of $g = 0$ μm, and the transmitted light is less, as summarized by the results in Fig. 13. Consequently, the electric field enhancement between the spheres facilitates the EOT in the mid-IR region.

To clarify which part of the substrate the light passed through, we also present electric field distribution profiles at substrate surface ($z = 0$) in Fig. 17. The profiles of Au-SiO_2 microsphere monolayers forming a square lattice (a) and a hexagonal lattice (b) are presented. The microspheres are attached ($g = 0$ μm), and excited by light at a wavelength of 16 μm, polarizing in x direction. In both cases, the electric field is localized at the thin gold films diamond-shaped (a) and triangle (b). Hence, we conclude that light passes through the gaps between the Au-SiO_2 microspheres and passes through the thin gold films on the substrate.

Optics EXPRESS

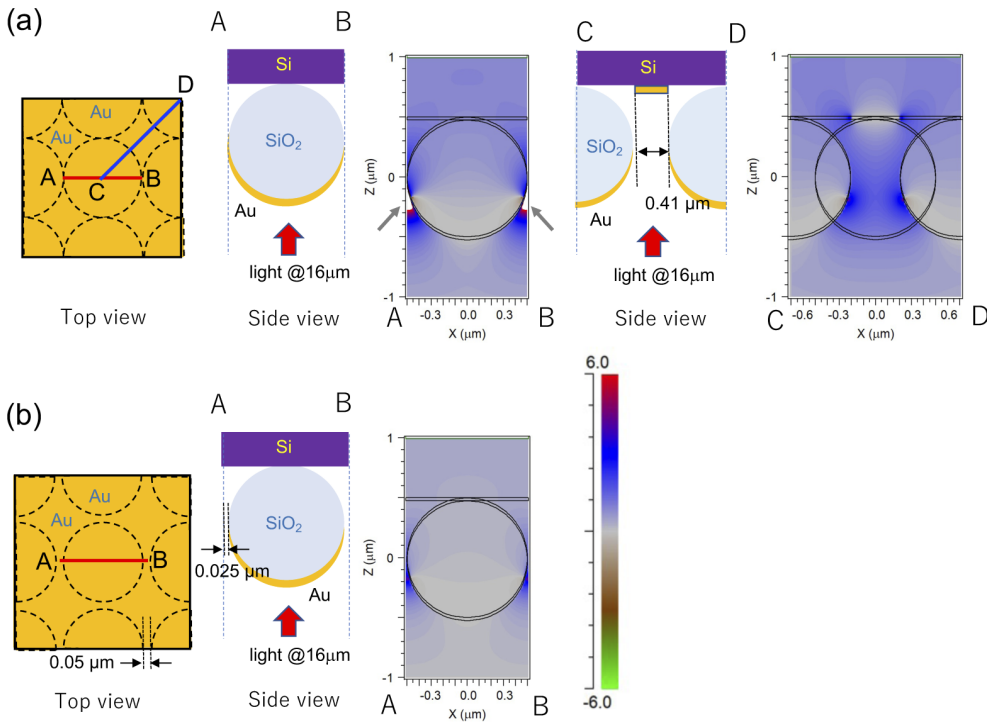

Fig. 16. (a) Electric field distribution profile of the Au-SiO_2 microsphere monolayer forming a square lattice, where the microspheres are attached ($g = 0$ μm), and excited by light at a wavelength of 16 μm. Both electric field distributions in the cut plane including AB and CD are illustrated. The white parts at the boundaries A and B represent the electric field grater than 6 (indicated by arrows). (b) Electric field distributions in the cut plane including AB, where the spheres are separated with gaps ($g = 0.05$ μm). For better understanding, the temporal change in the field distribution is provided in Visualization 1.

Optics EXPRESS

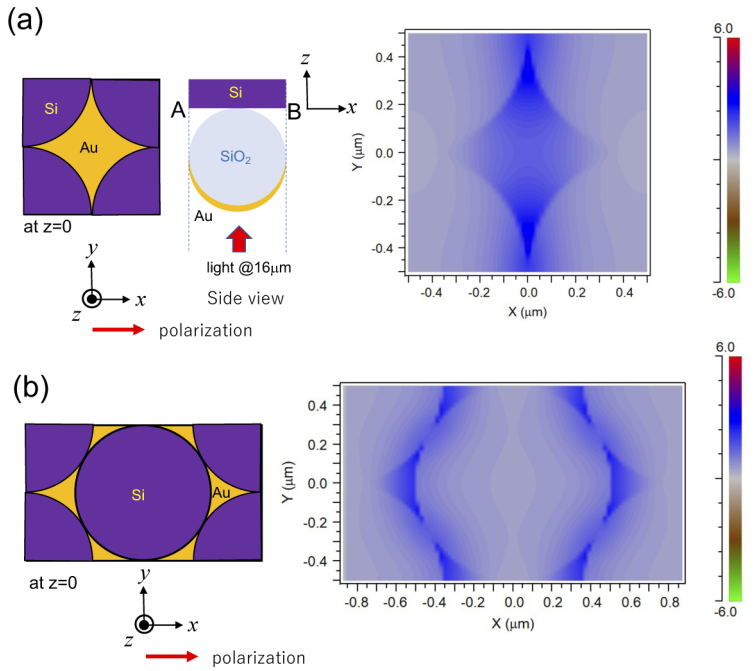

Fig. 17. (a) Electric field distribution profiles of the Au-SiO_2 microsphere monolayer forming a square lattice (a) and a hexagonal lattice (b), where the microspheres are attached ($g = 0$ μm), and excited by light at a wavelength of 16 μm. Both electric field distributions in the cut plane at $z = 0$, at the substrate surface. For better understanding, the temporal change in the field distribution is provided in Visualization 2.

4. Conclusion

We report EOT phenomena in Au-SiO_2- and Au-PS-microsphere monolayers in the mid-IR range from 5 to 25 μm. The observed transmittance is significantly greater than that of the flat gold film with the same thickness, although the surface of the Au-SiO_2 microsphere monolayer appears to be completely covered with gold films when observed from above. The FDTD calculation indicates that light passes through the openings between the gold film on the substrate surface and the gold cap. The EOT occurs in a wide wavelength range of the mid-IR, indicating that the EOT is not attributed to the resonance of the surface plasmons in a metal. This type of EOT is absent in the visible and near-IR wavelength range, where gold does not function as an ideal metal. In addition, spectral modification stemming from LPhPR in silica microsphere is also observed. The LPhPR can be interpreted based on the analogy of the localized surface plasmon resonance in metallic nanospheres, in the visible light or ultraviolet wavelength range.

Funding. Japan Society for the Promotion of Science (16K13696, 19H02624, 26286058).

Disclosures. The authors declare no conflicts of interest.

Data availability. Data underlying the results presented in this paper are not publicly available at this time but may be obtained from the authors upon reasonable request.

References

1. R. P. Van Duyne, J. C. Hulteen, and D. A. Treichel, "Atomic force microscopy and surface-enhanced Raman spectroscopy. I. Ag island films and Ag film over polymer nanosphere surfaces supported on glass," J. Chem. Phys. **99**(3), 2101–2115 (1993).

Optics EXPRESS

2. W.-H. Yang, J. Hulteen, G. C. Schatz, and R. P. Van Duyne, "A surface enhanced hyper Raman and surface enhanced Raman scattering study of trans 1, 2-bis(4 -pyridyl)ethylene adsorbed onto silver film over nanosphere electrodes. Vibrational assignments: Experiment and theory," J. Chem. Phys. **104**(11), 4313–4323 (1996).
3. L. A. Dick, A. D. McFarland, C. L. Haynes, and R. P. Van Duyne, "Metal film over nanosphere (MFON) Electrodes for surface-enhanced raman spectroscopy (SERS): Improvements in surface nanostructure stability and suppression of irreversible loss," J. Phys. Chem. B **106**(4), 853–860 (2002).
4. K. E. Shafer-Peltier, C. L. Haynes, M. R. Glucksberg, and R. P. Van Duyne, "Toward a Glucose Biosensor Based on Surface-Enhanced Raman Scattering," J. Am. Chem. Soc. **125**(2), 588–593 (2003).
5. X. Zhang, M. A. Young, O. Lyandres, and R. P. Van Duyne, "Rapid detection of an anthrax biomarker by surface-enhanced Raman spectroscopy," J. Am. Chem. Soc. **127**(12), 4484–4489 (2005).
6. M. Himmelhaus and H. Takei, "Cap Shaped gold nanoparticles for an optical biosensor," Sens. Actuators, B **63**(1-2), 24–30 (2000).
7. H. M. Hiep, T. Nakayama, M. Saito, S. Yamamura, Y. Takamura, and E. Tamiya, "A Microfluidic Chip Based on Localized Surface Plasmon Resonance for Real-Time Monitoring of Antigen-Antibody Reactions," Jpn. J. Appl. Phys. **47**(2), 1337–1341 (2008).
8. D. K. Kim, S. M. Yoo, T. J. Park, H. Yoshikawa, E. Tamiya, J. Y. Park, and S. Y. Lee, "Plasmonic properties of the multispot copper-capped nanoparticle array chip and its application to optical biosensors for pathogen detection of multiplex DNAs," Anal. Chem. **83**(16), 6215–6222 (2011).
9. M. Toma and K. Tawa, "Plasmonic coloration of silver nanodome arrays for a smartphone-based plasmonic biosensor," Nanoscale Adv. **1**(9), 3699–3708 (2019).
10. M. Toma, R. Tanaka, and K. Tawa, "Size effect of metal nanodome arrays on performance of plasmonic biosensor," Jpn. J. Appl. Phys. **59**(SD), SDDF03 (2020).
11. C. Farcau, "Metal-coated microsphere monolayers as surface plasmon resonance sensors operating in both transmission and reflection modes," Sci. Rep. **9**(1), 3683 (2019).
12. H. Kwona, S. Ryu, S. Lee, and S. Kim, "A fully biocompatible poly(ethylene glycol) gold plasmonic crystal for optical sensing," Opt. Mater. **47**, 333–337 (2015).
13. S. J. Peppernick, A. G. Joly, K. M. Beck, W. P. Hess, J. Wang, Y.-C. Wang, and W. D. Wei, "Photoemission electron microscopy of a plasmonic silver nanoparticle trimer," Appl. Phys. A **112**(1), 35–39 (2013).
14. H. Takei, "Surface-adsorbed polystyrene spheres as a template for nanosized metal particle formation: optical properties of nanosized Au particle," J. Vac. Sci. Technol., B: Microelectron. Process. Phenom. **17**(5), 1906–1911 (1999).
15. H. Takei, M. Himmelhaus, and T. Okamoto, "Absorption spectrum of surface-bound cap-shaped gold particles," Opt. Lett. **27**(5), 342–344 (2002).
16. C. A. Tira, I. Ly, R. A. L. Vallee, S. Astilean, and C. Farcau, "Shaping light spectra and field profiles in metal-coated monolayers of etched microspheres," Opt. Mater. Express **7**(8), 2847–2859 (2017).
17. C. Farcau, M. Giloan, E. Vinteler, and S. Astilean, "Understanding plasmon resonances of metal-coated colloidal crystal monolayers," Appl. Phys. B **106**(4), 849–856 (2012).
18. T. Endo, H. Takizawa, Y. Imai, Y. Yanagida, and T. Hatsuzawa, "Study of electrical Field distribution of gold-capped nanoparticle for excitation of localized surface plasmon resonance," Appl. Surf. Sci. **257**(7), 2560–2566 (2011).
19. R. Fujimura, R. Zhang, Y. Kitamoto, M. Shimojo, and K. Kajikawa, "Modeling of semi-shell nanostructures formed by metal deposition on dielectric nanospheres and numerical evaluation of plasmonic properties," Jpn. J. Appl. Phys. **53**(3), 035201 (2014).
20. T. W. Ebbesen, H. J. Lezec, H. F. Ghaemi, T. Thio, and P. A. Wolff, "Extraordinary optical transmission through sub-wavelength hole arrays," Nature **391**(6668), 667–669 (1998).
21. W. L. Barnes, A. Dereux, and T. W. Ebbesen, "Surface plasmon subwavelength optics," Nature **424**(6950), 824–830 (2003).
22. F. J. Garcia-Vidal, L. Martin-Moreno, T. W. Ebbesen, and L. Kuipers, "Light passing through subwavelength apertures," Rev. Mod. Phys. **82**(1), 729–787 (2010).
23. J. A. Hutchison, D. M. O'Carroll, T. Schwartz, C. Genet, and T. W. Ebbesen, "Absorption-induced transparency," Angew. Chem., Int. Ed. **50**(9), 2085–2089 (2011).
24. L. Landstroem, D. Brodoceanu, D. Baeuerle, F. J. Garcia-Vidal, S. G. Rodrigo, and L. Martin-Moreno, "Extraordinary transmission through metal-coated monolayers of microspheres," Opt. Express **17**(2), 761–772 (2009).
25. A. M. M. Gherman, A. Vladescu, A. E. Kiss, and C. Farcau, "Extraordinary optical transmission through titanium nitride-coated microsphere lattice," Photonics Nanostructures: Fundam. Appl. **38**, 100762 (2020).
26. D.-Z. A. Chen, R. Hamam, M. Soljačič, J. D. Joannopoulos, and G. Chen, "Extraordinary optical transmission through subwavelength holes in a polaritonic silicon dioxide film," Appl. Phys. Lett. **90**(18), 181921 (2007).
27. W. S. Rasband, "ImageJ, U. S. National Institutes of Health, Bethesda, Maryland, USA," https://imagej.nih.gov/ij/ (1997-2018).
28. C. A. Schneider, W. S. Rasband, and K. Eliceiri, "NIH Image to ImageJ: 25 years of image analysis," Nat. Methods **9**(7), 671–675 (2012).
29. M. D. Abramoff, P. J. Magalhaes, and S. J. Ram, "Image Processing with ImageJ," Biophotonics International **11**, 36–42 (2004).

Optics EXPRESS

30. I. H. Malitson, "Interspecimen Comparison of the Refractive Index of Fused Silica," J. Opt. Soc. Am. **55**(10), 1205–1209 (1965).
31. R. Kitamura, L. Pilon, and M. Jonasz, "Optical constants of silica glass from extreme ultraviolet to far infrared at near room temperature," Appl. Opt. **46**(33), 8118–8133 (2007).
32. T. L. Myers, R. G. Tonkyn, T. O. Danby, M. S. Taubman, B. E. Bernacki, J. C. Birnbaum, S. W. Sharpe, and T. J. Johnson, "Accurate measurement of the optical constants n and k for a series of 57 inorganic and organic liquids for optical modeling and detection," Appl. Spectrosc. **72**(4), 535–550 (2018).
33. https://refractiveindex.info.
34. R. L. Olmon, B. Slovick, T. W. Johnson, D. Shelton, S.-H. Oh, G. D. Boreman, and M. B. Raschke, "Optical dielectric function of gold," Phys. Rev. B **86**(23), 235147 (2012).
35. T. R. Steyer, K. L. Day, and D. R. Huffman, "Infrared Absorption by Small Amorphous Quartz Spheres," Appl. Opt. **13**(7), 1586–1590 (1974).
36. K. Kiyota and K. Kajikawa, "Effective medium and equivalent circuit analysis of extraordinary transmission through metallic grating in the infrared range," OSA Continuum **2**(5), 1639–1651 (2019).